American Journal of Modeling and Optimization, 2016, Vol. 4, No. 1, 13-18
Available online at http://pubs.sciepub.com/ajmo/4/1/2

DOI:10.12691/ajmo-4-1-2

An Optical and Electrical Modeling of Dye Sensitized Solar Cell: Influence of the Thickness of the Photoactive Layer

El Hadji Oumar Gueye*, Papa Douta Tall, Cheikh Birahim Ndao, Alle Dioum, Abdoulaye Ndiaye Dione, Aboubaker Chedikh Beye

Groupe Laboratoire Physique du Solide et Sciences des Materiaux, Physics Department, Cheikh Anta Diop University, Dakar, Senegal
*Corresponding author: elhadjioumar1.gueye@ucad.edu.sn

Abstract Dye sensitized solar cells (DSSC) are used for photovoltaic applications. The paper presents a methodology for optical and electrical modeling of dye-sensitized solar cells (DSSCs). In order to take into account the scattering process, the optical model is based on the determination of the effective permittivity of the mixture and the scattering coefficient using Mie and Bruggeman theories, considering spherical particles. Then, from the radiative transfer equation, the optical generation rate of cell is deduced. Coupling the output of the optical model (the dye generation rate) to an electrical model for charge generation, transport, and first-order (linear) recombination, allows determination of current density and maximum power output. Due to our model, the dependence effects of the thickness of the photoactive layer upon the optical generation rate, the short circuit photocurrent density and the maximum power output are evidenced. Moreover, we see that when the thickness of the photoactive layer increases the optical generation rate increases. While, the short circuit current density and the maximum power output increase until d =10 µm then remain constant. Thereby, it was found that 10 µm of thickness is enough for the best I-V characteristics. Our results agree with those found in the literature.

Keywords: *Dye sensitized solar cell, Bruggeman Theory, Mie Theory, Radiatives Transfers Equations, Mathematical Modeling, Matlab, Optical Generation Rate, Maximum Power Output, Thickness, Solar Cell*

Cite This Article: El Hadji Oumar Gueye, Papa Douta Tall, Cheikh Birahim Ndao, Alle Dioum, Abdoulaye Ndiaye Dione, and Aboubaker Chedikh Beye, "An Optical and Electrical Modeling of Dye Sensitized Solar Cell: Influence of the Thickness of the Photoactive Layer." *American Journal of Modeling and Optimization*, vol. 4, no. 1 (2016): 13-18. doi: 10.12691/ajmo-4-1-2.

1. Introduction

Dye sensitized solar cells (DSCs) as alternative to solar cells have been widely studied in recent years [1,2,3]. Record efficiencies of over 11% have been achieved with ruthenium-complex sensitizers on laboratory-scale devices. [4,5,6] Dye sensitized solar cell is a mixture of nanostructured films, a sensitizer and an electrolyte containing the mediator sandwiched between two electrodes: a conductive oxide as an anode and a counter electrode as cathode as depicted in Figure 1. The efficiency of absorption of the incoming light by the dye is one of the paramount parameters for the cell performance. Accordingly, the peculiar composition of the photoactive layer makes the dye-sensitized solar cells very complicated to establish an optoelectronic model. Indeed, it is composed of a mixture of three materials (titanium dioxide, dye molecules and tri-iodide ions immerged within the electrolyte) which could raise homogeneity problems.

Various optical [7,8], electrical [9-18] and optoelectronic model [19,20] have been developed.

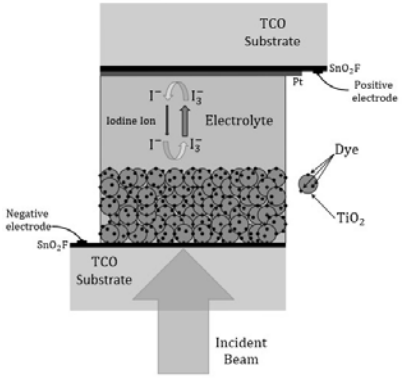

Figure 1. Structure of the Dye sensitized solar cell

In this paper, a coupled optical and electrical model of dye-sensitized solar cell will be presented, putting a focus on the accurate description of the optics in the photoactive layer (by applying Bruggeman's theory, Mie's Theory and radiative transfer equations). The influence of the thickness of the photoactive layer is also studied.

The paper is organized as follows. In the next section, we introduce the coupled optical and electrical model. The comparison of the simulation with the literature is reported

in the Results and Discussion section, which is followed by a Conclusions section.

2. Computational Model

The model considered is depicted in Figure 2. Thus, our study is essentially limited to the photoactive layer sandwiched between the two electrodes. The photoactive layer is a mixture of Titanium dioxide (TiO_2), a dye (Z907), a mediator and an electrolyte I^-/I_3^-.

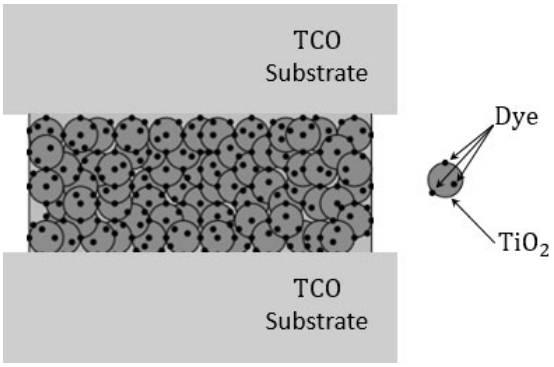

Figure 2. Schematic of the cell

2.1. Optical Model

By solving the equation of effective media (Equation 1), an analytical expression is obtained (equation 2, 3, 4):

$$X\frac{\varepsilon_a-\varepsilon_{Br}}{\varepsilon_a+2\varepsilon_{Br}}+(1-X)\frac{\varepsilon_b-\varepsilon_{Br}}{\varepsilon_b+2\varepsilon_{Br}}=0 \quad (1)$$

$$n_{Br}=\sqrt{\frac{m(\varepsilon_a,\varepsilon_b,X)+\sqrt{\begin{pmatrix}m(\varepsilon_a,\varepsilon_b,X)^2\\+n(\varepsilon_a,\varepsilon_b,X)^2\end{pmatrix}}}{2}} \quad (2)$$

$$k_{ext\,Br}=\frac{n(\varepsilon_a,\varepsilon_b,X)}{2n_{Br}} \quad (3)$$

$$\varepsilon_{Br}=n_{Br}^2-k_{Br,ext}^2+2ik_{Br,ext}n_{Br} \quad (4)$$

where ε_a and ε_b are the permittivity of the particles a and b, ε_{Br} the effective permittivity and, X filling fraction of particle (a and b were TiO_2 or dye and/or mediator) following the case considered.

In order to apply the Bruggeman theory [21], as done by Rothenberger et al. [8], TiO_2 particles are supposed to be in a spherical shape, as well as the dye molecules, and the mixture electrolyte + mediator.

This previous theory is used in two different ways. One is a mixture of TiO_2 and dye and the other is a mixture of a {(nanostructured film+ dye) & (electrolyte+ mediator)}.

The filling fraction of each individual component will be determined. For the mix of TiO_2 particle + dye the filling fraction of each individual component will be determined as follows:

We consider a diamond structure. Each TiO_2 particle admits four neighbors (coordination number CN = 4) [22,23]. The area occupied by the dye is given by the surface area of a sphere minus the reduction of surface area $CN\Delta S$. Meng et al [24] calculated the reduction of the surface area. His method will allow us to take into account the overlap distance h in our calculation. In fact, ΔS is function of the overlap distance h, equal to $r_{TiO2}/100$, with r_{TiO2} is the TiO_2 radius.

$$S_{colorant}=4\pi r^2-CN\Delta S \quad (5)$$

The number of dye is then deduced, assuming that each dye is a sphere of radius 1 nm. Thus, volumes (dye and TiO_2) are calculated and their filling fractions deducted. After determining the filling fractions, the effective permittivity of TiO_2-dye mixture is determined using equations (2), (3) and (4).

In the case of the mixture (TiO_2 +dye) / (electrolyte +mediator), the filling fraction of the electrolyte +mediator is equal to the porosity. Therefore, we determine the porosity.

We define the system as follows: First, the radius of all the nanoparticles are equal. Colloids considered perfectly spherical. The penetration length for two neighboring particles thus given by:

$$d_p=2r(1-h) \quad (5)$$

With d_p: distance between nanoparticles, r: radius of the sphere, h: the overlap distance.

Equation (5) can visualized in Figure 3.

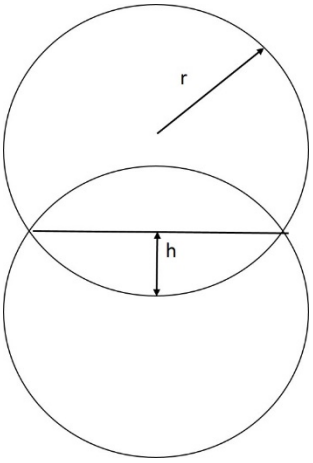

Figure 3. Schematic picture of the overlap between two particles

Taylor et al's equations are used to determine the porosity [25,26]. In these equations, the porosity is deduced by determining the volume of a single cell and the solid volume (sphere in our case) in this single cell.

The volume of the single cell is a function of the packing factor and diameter of the sphere. The volume is:

$$V=\alpha_m d^3 \quad (6)$$

α_m: packing factor, d: diameter of the sphere.

With the volume of the single cell known, the calculation of the porosity requires the determination of the total volume of the sphere in the single cell. For this calculation, Taylor et al based themselves on the calculations of Deb [27]. It determines the volume of a sphere taking into account the overlapping surface between the spheres. Thus, the volume of the sphere in the single cell is:

$$V_b=\frac{\pi}{6}(d+2h)^3-CN\frac{\pi}{3}h^3\left[3\left(\frac{d}{2}+h\right)-h\right] \quad (7)$$

h: overlap distance; CN: coordination number.

The first term on the right corresponds to the total volume of the sphere. The second term corresponds to the sum of the volumes of each spherical cape. Taylor et al. [25-26] used equations for the volume of single cell (6), the volume of sphere (7), and then obtained the following equation for the calculation of the porosity of a cell containing a number n of spheres

$$P = 1 - \frac{n\pi}{\alpha_m}\left[\frac{2-CN}{12}\left(\frac{2h}{d}\right)^3 + \frac{4-CN}{8}\left(\frac{2h}{d}\right)^2 \frac{1}{2}\left(\frac{2h}{d}\right) + \frac{1}{6}\right] \quad (8)$$

We will calculate the porosity for a diamond-like structure using equation (8) and Table 1. Thus, with the overlap distance h, equal to $r_{TiO2}/100$, we found P=0.64. The result of porosity agree with those found in literature. [19,22,23].

After determining the porosity, the filling fractions are deduced. Thus, the effective permittivity of the photoactive layer (TiO_2-dye + electrolyte-mediator) is calculated using equations (2), (3) and (4).

Table 1

Structure	Coordination number	Number of spheres by unit cell	Packing factor α_m
Diamond	4	8	12.35

After determining the effective permittivity of the mixture, the extinction, diffusion and absorption coefficients (σ) and the extinction, diffusion and absorption efficiencies will be calculated using Mie theory [28].

These results are used to calculate the macroscopic scattering coefficient and the macroscopic absorption coefficient (equations 10 and 11). In this approach, we assume that only the dyes are involved in the absorption process. The electrolyte + mediator couple absorbs only in the short wavelengths. TiO_2 does not absorb in this wavelength range [19]. In the scattering process, only the molecules of TiO_2 and electrolyte + mediator couple involved. The size of the dyes is very low [7], and therefore does not easily scatters.

$$K = \sigma_{abs} \times n_{abs} \quad (9)$$

$$S = \sigma_{scat} \times n_{scat} \quad (10)$$

These results are inserted in the radiatives transfer equation (4 flux) [29] to determine the expression of different flows. These expressions will be used for determining the absorption rate. The variation of these fluxes is gave by the following equations:

$$\frac{dI_c(x)}{dx} = (K+S)I_c(x) \quad (11)$$

$$\frac{dJ_c(x)}{dx} = -(K+S)J_c(x) \quad (12)$$

$$\frac{dI_d(x)}{dx} = \gamma K I_d(x) + \gamma(1-\zeta)SI_d(x) - \gamma(1-\zeta)SJ_d(x) - \zeta SI_c(x) - (1-\zeta)SJ_c(x) \quad (13)$$

$$\frac{dJ_d(x)}{dx} = -\gamma K J_d(x) - \gamma(1-\zeta)SJ_d(x) + \gamma(1-\zeta)SI_d(x) + (1-\zeta)SI_c(x) + \zeta x I_c(x) \quad (14)$$

The factor γ is the equivalent path length for diffuse flows (I_d, J_d). Roze et al. [30] give the analytical expression of the forward scattering ratio (ζ). The four flow I_c, I_d, J_c and I_d are determined taking into account the following boundary conditions.

At the interface Glass / Mixed Zone

$$I_c(a) = (1-r_c)I_c^a + r_c J_c(a) \quad (15)$$

$$I_d(a) = (1-r_d)I_d^a + r_d J_d(a) \quad (16)$$

where r_c , r_d , r_c^b , r_d^b the reflective coefficient of collimated beam, the reflective coefficient of radiation diffuse beam, the reflective coefficient of collimated beam at the back, the reflective coefficient of radiation diffuse beam at back side respectively.

I_c^a and I_d^a are collimated incident flux and the incident flux diffused at the interface x = a. I_c^a is determined taking into account the effects of reflection at interfaces (glass interface / mixed zone and air / glass) and is given by:

$$I_c^a = \frac{\left(1-r_c^b\right)}{1-\left(r_c^b r_c\right)} I_0 \quad (17)$$

Here $I_d^a = 0$; I_0=incident light.

At the interface mixed zone / Glass: x = 0.

Considering the effects of reflection at interfaces (air / glass and glass / mixed zone), the following conditions are given:

$$J_c(0) = \left[\frac{r_c\left(1-2r_c^b\right)+r_c^b}{1-r_c r_c^b}\right] I_c(0) \quad (18)$$

$$J_d(0) = \left[\frac{r_d^b\left(1-2r_d\right)+r_d^i}{1-r_d^b r_d}\right] I_d(0) \quad (19)$$

Thus, the local absorption rate per unit volume [8] established using the following expression:

$$g(x) = KI_c(x) + KJ_c(x) + \gamma KI_d(x) + \gamma KJ_d(x) \quad (20)$$

The optical photons absorption rate can then be deduced from g (x) [31]:

$$G_a(x) = \frac{g(x)}{\frac{hc}{\lambda}} \quad (21)$$

Finally, the optical photogeneration rate of the DSC given by:

$$G(x) = G_a(x) \times \eta \quad (22)$$

Where η is the injection rate.

2.2. Electrical Model

The charge generation function $G_e(x) = \eta_{inj} G_{dye}(x)$, is coupled to an electrical model for free charge carriers. Here, for simplicity, we do not include ionic transport in the electrolyte and the reduction of triiodide at the counter-electrode. The electrical model is based on the stationary continuity equation. We suppose that there is no trapping states, i.e the electron is only in the conduction band of the TiO_2 layer. A purely diffusive transport equation for the electrical current density J is taken. [9] Then, in the ideal model case, only electrons from the conduction band can recombine with triiodide in the electrolyte, and the recombination rate is taken to be first order in n(x)(n(x): carriers density). This leads to an inhomogeneous linear differential equation for n(x)

$$L^2 \frac{d^2 n(x)}{dx^2} - [n(x) - n_0] + \tau_0 G_e(x) = 0 \qquad (23)$$

Here, $L = \sqrt{\tau_0 D_0}$ is the constant electron diffusion length, τ is the electron lifetime, and n_0 is the electron number density at equilibrium in the dark. The electron number density in the dark n_0 is given by

$$n_0 = N_c e^{(E_{F0} - Ec)/k_B T} \qquad (24)$$

where N_c is the effective density of the conduction band states, E_c is the conduction band energy, and E_{F0} is the Fermi level in the dark, which is equilibrated with the redox potential of the iodide/triiodide couple.

Based on both modeling and experimental results, effect of porosity (P) on the diffusion coefficient (D_0) can be expressed as

$$D_0 = a|P - P_c|^{\mu} \text{ [32]} \qquad (25)$$

where the constants a and μ, and the critical porosity Pc are $4.10^{-4} cm^2 s^{-1}$, 0.82 and 0.76, respectively.

The boundary conditions to equation 23 are

$$n(x = 0) = n_0 e^{qV/k_B T} \qquad (26)$$

And

$$\left.\frac{dn}{dx}\right|_{x=d} = 0 \qquad (27)$$

where V is the photovoltage.

The general solution of (23) is given by

$$n(x) = n_h(x) + n_p(x) \qquad (28)$$

Here

$$n_h(x) = Ee^{x/L} + Fe^{-x/L} \qquad (29)$$

$$n_p(x) = n_1(x) + n_2(x) + n_3(x) + n_4(x) \qquad (30)$$

$$n_1(x) = Ie^{ax},\ n_2(x) = Je^{-ax},\ n_3(x) = Ke^{bx},\ n_4(x) = Me^{-bx} \qquad (31)$$

Where E and F are constants determined by the boundary conditions. I, J K and M function of the generation rate. From the complete solution for V = 0, the photocurrent density at short circuit can be calculated by

$$J_{sc} = eD_0 \left.\frac{dn}{dx}\right|_{x=0} \quad \text{for V} = 0. \qquad (32)$$

3. Results and Discussions

The analytical model presented above is validated with experimental data reported in the literature (Figure 4, Figure 5).

We make here (Figure 4) a comparison between our results and those of Wenger et al. [19] Here we see that for the same radii (r = 20 nm); we have almost the same values, but with different paces. When we the radius is 40 nm the paces are almost the same. This can explained by the fact that Wenger et al extracted the coefficients experimentally and the radius are rarely homogeneous [33] in that case, which may be the cause of our differences.

The analytical model presented above validated with experimental data reported in the literature. The modeling of solar cell performance in terms of short-circuit photocurrent is compared with the experimental measurements reported by Saito et al. [34] (Figure 5). The normalized modeling and experimental results plotted in Figure 5 show a good agreement. These results show also a good agreement with other result in literature [35].

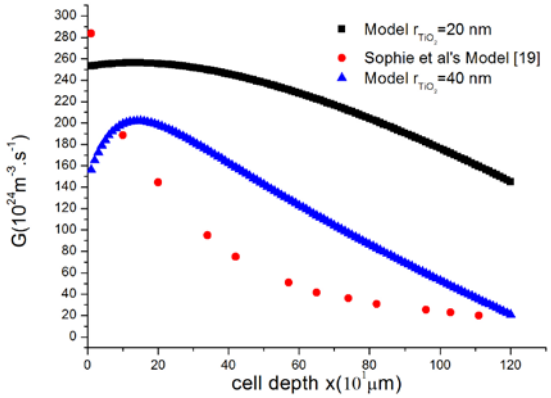

Figure 4. the generation rate of the dye depending on the depth of the cell

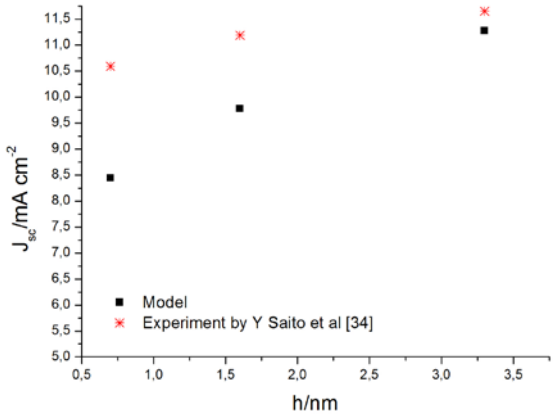

Figure 5. Short circuit photocurrent density as a function of overlap distance

Figure 6 shows the generation rate as a function of the thickness of the photoactive layer d. We see that when d

increases the generation rate increase. In fact, the TiO_2 particles increase and then the dye molecules.

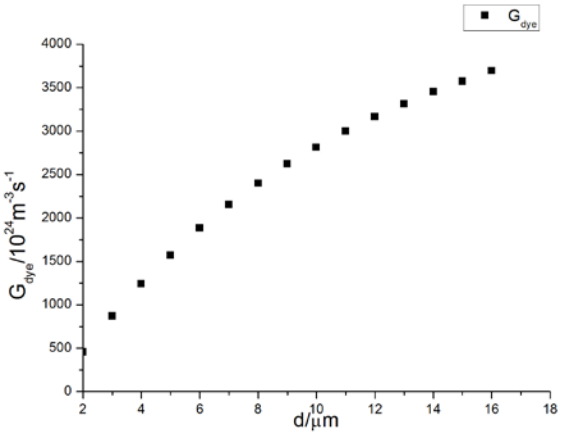

Figure 6. generation rate as a function of the thickness of the photoactive layer

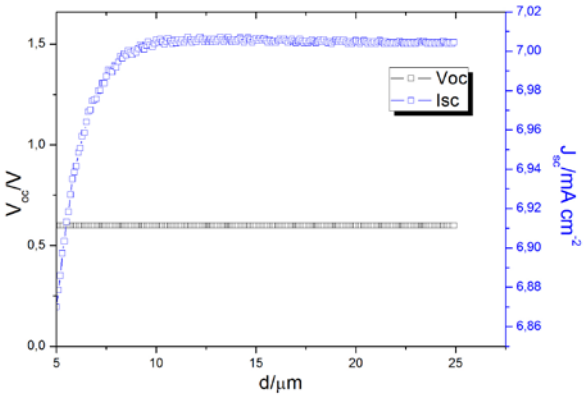

Figure 7. open circuit photo-voltage V_{oc} and short-circuit photocurrent density J_{sc} as a function of the thickness of the photoactive layer

Figure 7 shows the open circuit photo-voltage V_{oc} and short-circuit photocurrent density J_{sc} as a function of the thickness of the photoactive layer. We see that, when the thickness increases, J_{sc} increases until d=10 µm then remain constant. However, V_{oc} remains constant, which aggre well with the result found on literature. [36] The constant value of V_{oc} is attributed -according to Park et al [36]- to the compensating effect associated with the dependence of the number of dye molecules and recombination centers on the surface area.

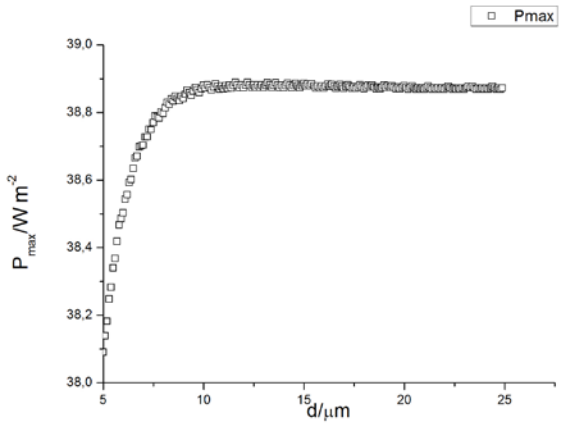

Figure 8. Maximum power output as a function of the thickness of the photoactive layer

Then, in Figure 8, we see that when d increases the maximum power output P_{max} increases until d=10 µm but remains practically constant after 10 µm. Therefore, according to our model, a thickness 10 µm is adequate for a good efficiency of dye-sensitized solar cell. This result agree well with those found on literature. [36,37] Indeed, Huang et al [37], show that for a good efficiency, a thickness of 12 µm of TiO_2 film is adequate.

4. Conclusion

Our model allows us to see the influence of the thickness of the photoactive layer d on the generation rate, the short circuit current density I_{sc}, the open circuit voltage V_{oc} and the maximum power output P_{max}.

Thus, we see that when the thickness of the photoactive layer d, the generation rate increases. However, I_{sc} and P_{max} increase until d=10 µm, then remain constant. While, V_{oc} remains constant.

Then, according to our model, a thickness of 10 µm is enough for a dye-sensitized solar cell with good characteristics. Our results agree with the ones found in the literature.

However, this model has some limitation: the particles are not necessarily spherical and of the same size and the difference between the reflected coefficient diffused and collimated could be taken into account for better precision.

References

[1] O'Regan, B., Grätzel, M., "A low-cost, high-efficiency solar cell based on dye-sensitized colloidal TiO_2 films," *Nature*, 353-737, 1991.

[2] Wang, Q., Ito, S., Gratzel, M., Fabregat-Santiago, F., Mora-Sero, I., Bisquert, J., Bessho, T., and Imai, H., "Characteristics of High Efficiency Dye-Sensitized Solar Cells," *J. Phys. Chem.* B 110, 25210-25221, 2006.

[3] Mathew, S., Yella, A., Gao, P., Humphry-Baker, R., Curchod, B.F.E., Tavernelli, I., Rothlisberger, U., Nazeeruddin M.K., and Grätzel, M., "Dye-sensitized solar cells with 13% efficiency achieved through the molecular engineering of porphyrin sensitizers," *Nature Chemistry 6*, 242-247, 2014.

[4] Green, M. A., Emery, K., Hishikawa, Y., Warta, W., and Dunlop, E. D., "Solar cell efficiency tables (Version 45)," *Progress in photovoltaics: research and applications*, 23(1), 1-9, 2015.

[5] Chiba, Y.; Islam, A.; Watanabe, Y.; Komiya, R.; Koide, N.; Han, L., *J. Appl. Phys., Part 2*, 45, L638-L640, 2006.

[6] Gao, F.; Wang, Y., Shi, D., Zhang, J., Wang, M. K., Jing, X. Y., Humphry-Baker, R., Wang, P., Zakeeruddin, S. M., Grätzel, M., *J. Am. Chem. Soc.* 130, 10720-10728 ,2008.

[7] Ferber, J., and Luther, J., "Computer simulations of light scattering and absorption in dye-sensitized solar cells." *Solar Energy Materials and Solar Cells* 54 (1998).

[8] Rothenberger, G., Comte, P., Gratzel, M., "A contribution to the optical design of dye_sensitized nanocrystalline solar cells," *Solar Energy Materials & Solar Cells*, 58, 321-336, 1999.

[9] Soedergren, S., Hagfeldt, A., Olsson, J., and Lindquist, S. E., "Theoretical models for the action spectrum and the current-voltage characteristics of microporous semiconductor films in photoelectrochemical cells," *The Journal of Physical Chemistry*, 98(21), 5552-5556, 1994.

[10] Matthews, D., Infelta, P., and Grätzel, M, "Calculation of the photocurrent-potential characteristic for regenerative, sensitized semiconductor electrodes." *Solar Energy Materials and Solar Cells*, 44(2), 119-155, 1996.

[11] Ferber, J., Stangl, R., and Luther, J., "An electrical model of the dye-sensitized solar cell," *Solar Energy Materials and Solar Cells*, 53(1), 29-54, 1998.

[12] Usami, A., "Theoretical study of application of multiple scattering of light to a dye-sensitized nanocrystalline photoelectrichemical cell," *Chemical Physics Letters*, 277(1), 105-108, 1997.

[13] Usami, A., "Theoretical study of charge transportation in dye-sensitized nanocrystalline TiO_2 electrodes," *Chemical physics letters*, 292(1), 223-228, 1998.

[14] Ferber, J., Stangl, R., and Luther, J., "An electrical model of the dye-sensitized solar cell," *Solar Energy Materials and Solar Cells*, 53(1), 29-54, 1998.

[15] Stangl, R., Ferber, J., & Luther, J., "On the modeling of the dye-sensitized solar cell," *Solar Energy Materials and Solar Cells*, 54(1), 255-264, 1998.

[16] Usami, A., & Ozaki, H., "Computer simulations of charge transport in dye-sensitized nanocrystalline photovoltaic cells," *The Journal of Physical Chemistry B*, 105(20), 4577-4583, 2001.

[17] Bisquert, J., Cahen, D., Hodes, G., Rühle, S., & Zaban, A., "Physical chemical principles of photovoltaic conversion with nanoparticulate, mesoporous dye-sensitized solar cells," *The Journal of Physical Chemistry B*, 108(24), 8106-8118, 2004.

[18] Filipič, M., Berginc, M., Smole, F., & Topič, M., "Analysis of electron recombination in dye-sensitized solar cell," *Current Applied Physics*, 12(1), 238-246, 2012.

[19] Wenger, S., Schmid, M., Rothenberger, G., Gentsch, A., Gratzel, M., and Schumacher, J. O., "Coupled Optical and Electronic Modeling of Dye-Sensitized Solar Cells for Steady-State Parameter Extraction," *J. Phys. Chem. C* 115, 10218-10229, 2011.

[20] Topič, M., Čampa, A., Filipič, M., Berginc, M., Krašovec, U. O., & Smole, F., "Optical and electrical modelling and characterization of dye-sensitized solar cells," *Current Applied Physics*, 10(3), S425-S430, 2010.

[21] Berthier, S., and Lafait, J., "Modelisation des Propriétés Optiques des Milieux Inhomogènes a Structures Complexe," *Journal de Physique Colloque CI, supplément au N°1*, Tome 42, 1981.

[22] Fredin, K., Nissfolk, J., Hagfeldt, A., "Brownian dynamics simulations of electrons and ions in mesoporous films," *Solar Energy Materials & Solar Cells* 86, 283-297, 2005.

[23] Lagemaat, J., Benkstein, K., Frank, A., "Relation between Particle Coordination Number and Porosity in Nanoparticle Films: Implications to Dye-Sensitized Solar Cells," *The Journal of Physical Chemistry B* 105, 50, 2001.

[24] Meng, N., Michael, K.H., Dennis, Y.C., Leung, K., "An analytical study of the porosity effect on dye-sensitized solar cell performance," *Solar Energy Materials & Solar Cells*, 90, 1331-1344, 2006.

[25] Taylor, S. W. "Transport of substrate and biomass in porous media with application to in situ bioremediation of organic contaminants in groundwater," PhD thesis, Department of Civil Engineering, Princeton, 1990.

[26] Taylor, N.J., Milly, S.W., and Jaffe, P. R., "Biofilm growth and the related changes in the physical properties of a porous medium, 2, Permeability," *Water Resour. Res.*, 26(9), 2161-2169, 1990.

[27] Deb, A. K. "Theory of sand filtration." *J. Sanit. Eng. Div., ASCE,* 96(3), 399-422. (1969).

[28] C.F. Bohren, D.R. Huffman "*Absorption and scattering of light by small particles*," Wiley, 1998.

[29] Maheu, B., Letoulouzan, J.N., and Gouesbet, G., "Four-flux models to solve the scattering transfer equation in terms of Lorenz-Mie parameters," *Applied Optics*, 23 (19), 1984.

[30] Rozé, C., Girasole, T., Gréhan, G., Gouesbet, G., Maheu, B., "Four-flux models to solve the scattering transfer equation in terms of Lorenz-Mie parameters," *Optics communications* 194 251-263, 2001.

[31] Dioum, A, Ndiaye, S., Gueye, E.H.O., Gaye, M.B., Faye, D.N., Sakho, O., Faye, M., and Beye, A.C., "3-D Modeling of bilayer heterojunction organic solar cell based on Copper Phthalocyanine and Fullerene (CuPc/C60): evidence of total excitons dissociation at the donor-acceptor interface." *Global Journal of Pure and Applied Sciences*,19, 2013.

[32] Benkstein, K.D., Kopidakis, N., van de Lagemaat, J., Frank, A.J., "Influence of the Percolation Network Geometry on Electron Transport in Dye-Sensitized Titanium Dioxide Solar Cells," *Phys. Chem. B*, 107-114, 2003.

[33] Barbe, C.J., Arendse, F., Comte, P., Jirousck, M., Lenzmann, F., Shklover, V., Gratzel, M., "Nanocrystalline Titanium Oxide Electrodes for Photovoltaic Applications," *J. Am. Ceram. Soc*, 80, 31-57, 1997.

[34] Saito, Y., Kambe, S., Kitamura, T., Wada, Y., and Yanagida, S., "Morphology control of mesoporous TiO2 nanocrystalline films for performance of dye-sensitized solar cells," *Solar Energy Materials and Solar Cells*, 83(1), 1-13, 2004.

[35] Bisquert, J., and Marcus, R. A., "Device modeling of dye-sensitized solar cells. In: Multiscale Modelling of Organic and Hybrid Photovoltaics," *Springer Berlin Heidelberg*, 325-395, 2013.

[36] Park, N. G., Van de Lagemaat, J., and Frank, A. J., "Comparison of dye-sensitized rutile-and anatase-based TiO2 solar cells," *The Journal of Physical Chemistry B*, 104(38), 8989-8994, 2000.

[37] Huang, C. Y., Hsu, Y. C., Chen, J. G., Suryanarayanan, V., Lee, K. M., and Ho, K. C., "The effects of hydrothermal temperature and thickness of TiO2 film on the performance of a dye-sensitized solar cell," *Solar energy materials and solar cells*, 90(15), 2391-2397, 2006.